JOURNAL OF APPLIED ELECTROCHEMISTRY 24 (1994) 647–651

Electrochemical observation of instabilities of the Belousov–Zhabotinskii reaction in CSTR

K. KATAOKA, N. OHMURA, S. WATANABE, K. SUMIDA, S. DEKI

Department of Chemical Science and Engineering, Kobe University, Rokkodai-cho, Nadaku, Kobe 657, Japan

Received 10 May 1993; revised 16 August 1993

The instabilities of the Belousov–Zhabotinskii reaction were studied in an isothermal CSTR by varying the space velocity as bifurcation parameter. The time-dependent concentration of bromide ion and redox potential were observed, respectively, by a Ag–AgBr electrode and a platinum-wire electrode under reaction-controlling conditions. The single-peak periodic and the chaotic oscillations occur alternately with increasing space velocity. The multipeak oscillations were also observed at higher space velocities. Two kinds of chaotic oscillations were observed, chaotic oscillations with amplitudes varying irregularly in the periodic–chaotic sequence region and chaotic mixing of large and small amplitude in the multipeak oscillations region. An analysis of the phase portraits for these chaotic oscillations indicates that they correspond to low dimensional and fractal structures.

1. Introduction

Much attention has been paid recently to chaotic and self-organized phenomena in nonlinear systems. The Belousov–Zhabotinskii reaction (abbreviated the B–Z reaction) is known as one of such nonlinear chemical systems. In this reaction, malonic acid is oxidized by bromate ion in the presence of a metal catalyst in sulphuric acid solution. In an isothermal continuous stirred tank reactor (CSTR) the chemical species of this reaction oscillate in concentration. Schmitz *et al.* [1] and Hudson *et al.* [2, 3] observed various kinds of oscillations, including chaotic behaviours, at high feed flow rate. Turner *et al.* [4] and coworkers [5] investigated periodic–chaotic sequences at low flow rates, and they characterized time series data from the bromide-ion sensitive electrode record with power spectra and reconstructed attractors. The mechanistic source of chaos in this reaction, however, has not been elucidated because of the lack of reproduction of the various experiments: in particular at medium and high flow rates. Two reasons for the lack of reproduction are the strong nonlinearity due to a complex elementary reaction sequence and unavoidable external perturbations. In fact Schmitz *et al.* [1] recognize that any experimental system cannot avoid those perturbations. It is, therefore, difficult to ascertain by experiment whether the system would be truly chaotic in the absence of perturbation.

In the present work, an experiment was carried under isothermal, well-mixed condition with minimized external perturbations. The first purpose was to observe the transition of oscillation states in the wide range of the space velocity and to investigate a periodic–chaotic sequence. The second was to characterize chaotic behaviour and to ascertain whether the chaos appearing at medium and high space velocity is essential or not.

This paper was presented at the International Workshop on Electrodiffusion Diagnostics of Flows held in Dourdan, France, May 1993.

2. Experimental details

The four feeds were fed separately at an equal flow rate into a cylindrical glass vessel having a volume of $5.51 \times 10^{-5}\,m^3$ by means of four syringe pumps which can feed constantly without pulsation (Fig. 1). The mixed feed concentrations were the same as those employed by Hudson *et al.* [2, 3]: $0.30\,kmol\,m^{-3}$ malonic acid, $0.14\,kmol\,m^{-3}$ sodium bromate, $0.20\,kmol\,m^{-3}$ sulphuric acid and $0.1 \times 10^{-2}\,kmol\,m^{-3}$ ammonium cerium(III) nitrate. A small quantity of sodium bromide ($3.5 \times 10^{-6}\,kmol\,m^{-3}$) was added to the solution of ammonium cerium(III) nitrate. The reactor was maintained at constant temperature ($25 \pm 0.1^\circ C$). A Ag–AgBr electrode was used to measure the time-dependent concentration of bromide ion, and a platinium-wire electrode to measure the redox potential between Ce^{3+} and Ce^{4+}. A Ag–AgCl electrode served as the reference electrode. The stirring rate was 2300 r.p.m. so as to guarantee the system under reaction-controlling condition.

3. Results and discussion

3.1. *Time series and their spectra*

In the range $r = 2.78 \times 10^{-4} \sim 2.97 \times 10^{-3}\,s^{-1}$, a remarkable sequence of different dynamical regions, so-called periodic-chaotic sequence, was observed: periodic and chaotic oscillations occurred alternately, each existing over some range in r. The first region, which is called P_1, has single-peak periodic relaxation oscillations with very small amplitude. The amplitude of the oscillations tends to become

0021-891X

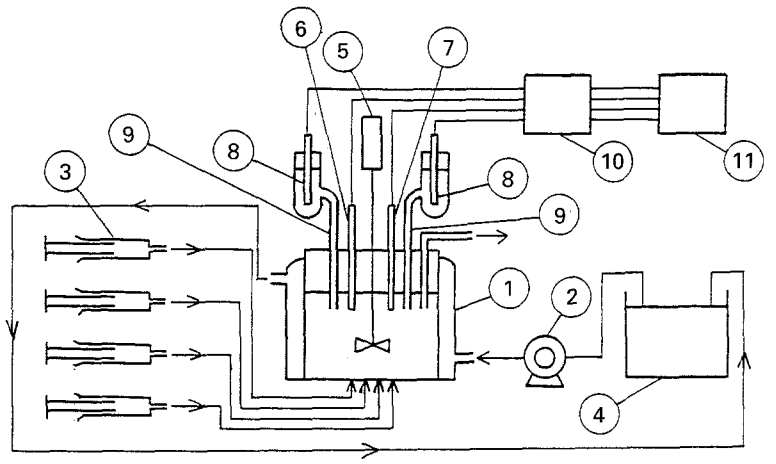

Fig. 1. Experimental setup. (1) Cylindrical glass reactor, (2) magnetic pump, (3) syringe pump, (4) constant temperature water tank with thermostat, (5) stirrer, (6) Ag–AgBr electrode, (7) Pt-wire electrode, (8) Ag–AgCl electrode immersed in saturated KCl solution, (9) saturated KNO_3 ager bridge, (10) data recorder and (11) millivolt recorder.

small with decreasing space velocity. This is due to the fact that this region is very close to chemical equilibrium. The second and the third periodic regions, called P_2 and P_3 respectively, also have single-peak periodic relaxation oscillations. The amplitudes in P_2 and P_3 are, however, larger than those in P_1. The relaxation oscillations have a few distinct time scales in one cycle. In these periodic regions, therefore, the spectrum consisted of a single fundamental frequency and its harmonics above the instrumental noise level, which seemed to have a complicated structure to some extent. Typical examples of a time trace and its spectrum in these periodic regions are shown in Fig. 2(a).

There were two chaotic regions (C_1, C_2) in the sequence. Both of the two chaotic regions were characterized by irregularly varying amplitudes. The spectrum becomes more complicated than that for

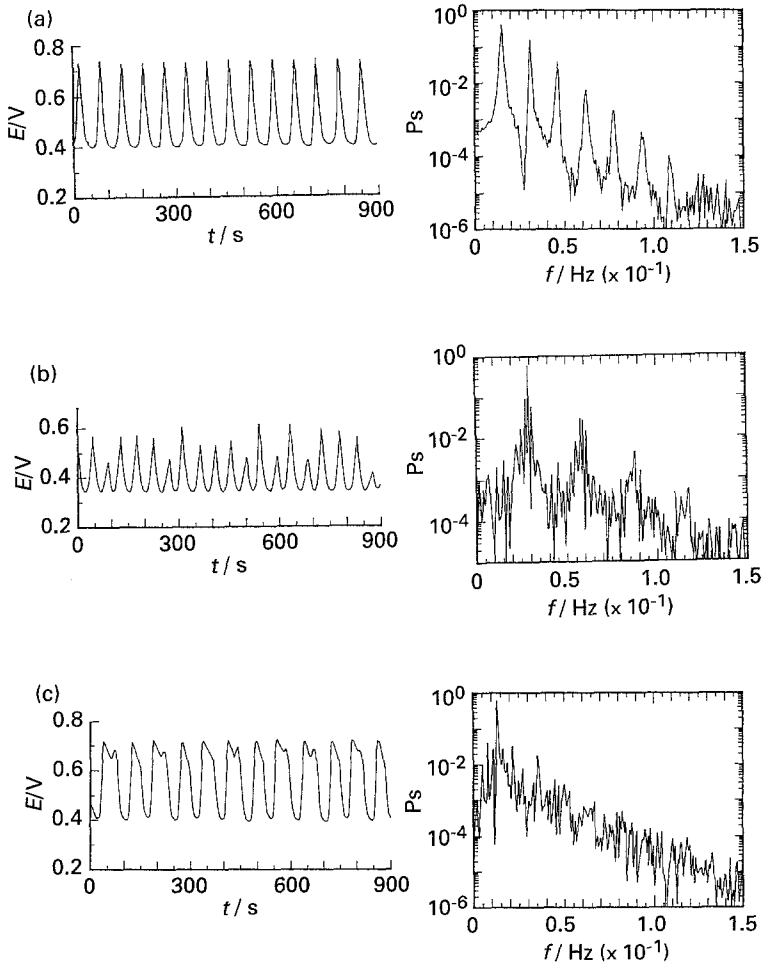

Fig. 2. Experimental results for three space velocities: (a) region P_2, $r = 5.54 \times 10^{-4}\ s^{-1}$, (b) region C_2, $r = 7.42 \times 10^{-4}\ s^{-1}$, (c) region M, $r = 3.67 \times 10^{-3}\ s^{-1}$. For each r the graph shows the oscillogram the Pt-wire electrode potential and the corresponding power spectrum. The general characteristics of the Ag–AgBr electrode output are essentially similar.

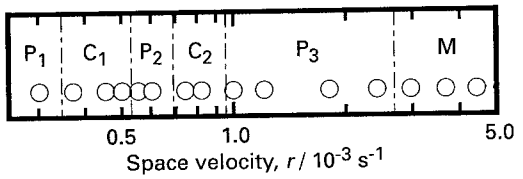

Fig. 3. The transition sequences given by experiment. The experimental data are shown by the circles.

periodic regions, and broad band noise arises (Fig. 2(b)). A similar sequence was observed by Turner *et al.* [3] and coworkers [4]. However, their periodic regions included multipeak oscillations which had in each period one large amplitude relaxation oscillation and some small amplitude sinusoidal oscillations. Therefore, the transition sequence that was observed in the present work is different from that reported by Turner *et al.* [3] and coworkers [4].

In the range $r = 2.97 \times 10^{-3} \sim 4.43 \times 10^{-3}\ s^{-1}$, multipeak oscillations were observed, which included chaotic states mixed with two different types of multipeak oscillations. (Multipeak oscillations region M.) It will be convenient to refer to resulting waveforms using the L^s notation [6], where L is the number of large-amplitude excursions and s is the number of small peaks in one cycle. The time trace and its power spectrum for the chaotic state mixed with 1^0 and 1^1 are shown in Fig. 2(c). These chaotic states were also characterized by broad band spectra, as Fig. 2(c) illustrates. From the point of the waveform and the spectrum structure, this sequence of multipeak oscillations states may be similar to that observed by Hudson *et al.* [2, 3] in approximately the same range of space velocity as this work. This result indicates that the present work reproduced qualitatively the experiment by Hudson *et al.* This sequence, however, could not be observed in detail in respect of the transition as Hudson *et al.* could do. This is because the syringe pumps were unable to change the feed rates slightly in the high flow rates. The sequence of regimes observed in the experiments is summarized in Fig. 3. Finally, at space velocity $r > 4.43 \times 10^{-3}\ s^{-1}$ the reaction state reached a dynamic equilibrium with no oscillation.

3.2. *Characterization of chaotic behaviours*

The chaotic behaviours in this reaction were characterized by the phase space portraits constructed from the redox potential time series which were embedded into m-dimensional phase space as $\{E(t), E(t+\tau), E(t+2\tau), \cdots, E(t+(m-1)\tau)\}$, where m is the embedding dimension and τ is a time delay [7, 8]. The time delay τ was arbitrarily fixed. Figure 4 shows two-dimensional chaotic phase portraits $E(t+\tau)$ against $E(t)$ and their Poincaré sections given by the intersection of orbits of three-dimensional phase portraits (where the third axis is $E(t+2\tau)$) with the $x = y$ plane. All Poincaré sections of these chaotic attractors seem to be nearly one-dimensional. These attractors, therefore, are almost two-dimensional in phase space. Judging from the structures of these attractors and Poincaré sections, the behaviours in the chaotic regions C_1 and C_2 seem to be the same type as those observed by Turner *et al.* [3] and coworkers [4], while the chaotic behaviours in the region of multipeak oscillations (M) seem to be the same type as those observed by Hudson *et al.* [3].

To quantify these chaotic attractors, the largest Lyapunov exponents of those chaotic data were estimated with the reliable method developed by Wolf *et al.* [9]. The largest Lyapunov exponent λ_{max} is plotted against space velocity in Fig. 5. The magnitudes of λ_{max} in the three periodic regions are approximately zero (0.00 ± 0.01), while those in the two chaotic regions are positive (more than 0.01). Wolf *et al.* [9] also estimated the chaotic data in this reaction system, and their estimation gave a result that λ_{max} was about 0.0054. In either case, λ_{max} values are very small. These results, therefore, indicate weak and low dimensional chaos.

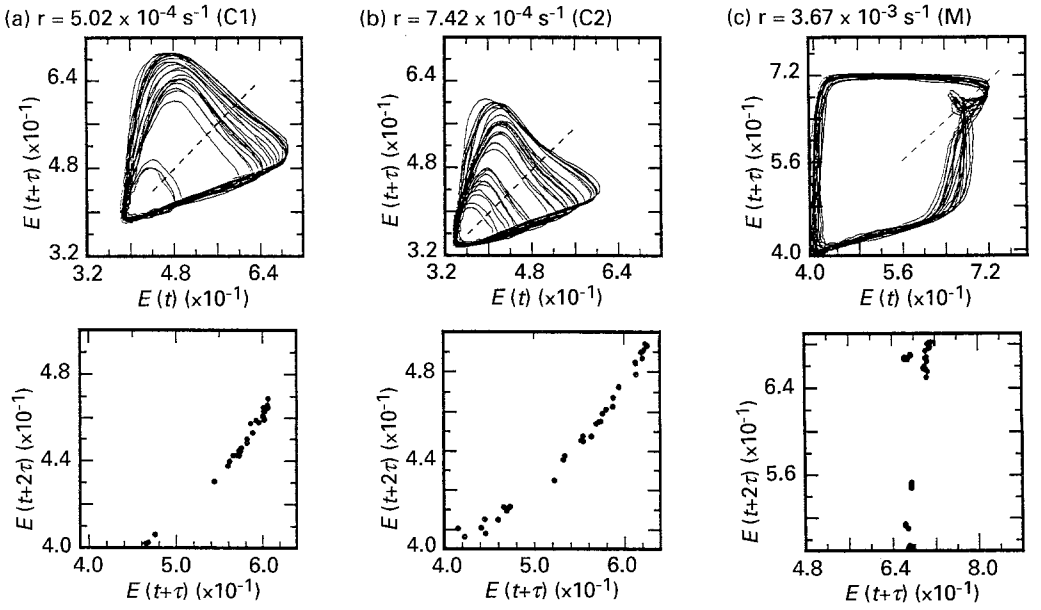

Fig. 4. Chaotic phase portraits and Poincaré sections. (Every time delay $\tau = 8$ s.)

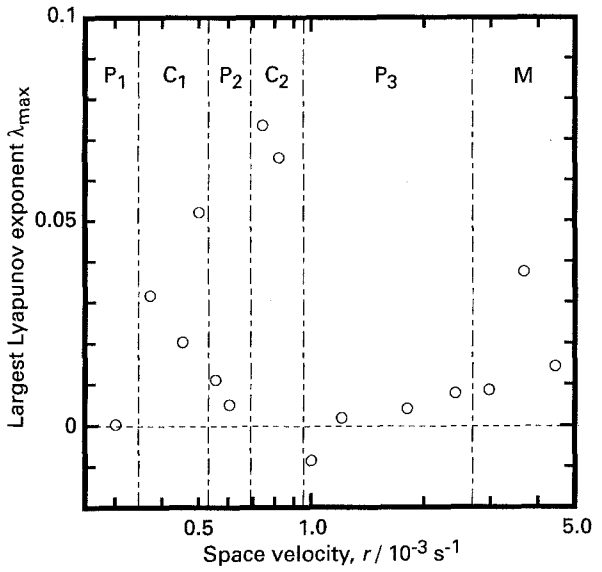

Fig. 5. The largest Lyapunov exponents against space velocity.

In chaos of dissipative dynamical systems, the volume of phase space reduces with time and finally it becomes zero. The strange attractor is, therefore, stretched in the direction of positive Lyapunov exponents and folded repeatedly due to its nonlinearity. As a result, the strange attractor has a complicated and self-similar structure like a Cantor set, i.e. fractal structure. The fractal dimension is a very important measure which characterizes the geometric feature of strange attractor in dissipative dynamical systems. There are several kinds of definition for the fractal dimension, and the correlation dimension proposed by Grassberger and Procaccia [10] was adopted. It is clear that the dimensions in chaotic regions are larger than those in periodic regions (Fig. 6). Moreover, the dimension is in a relatively good agreement with the corresponding largest Lyapunov exponent (compare with Fig. 5). The attractors of singly periodic regions are a limit cycle, so the dimensions of the attractors should be 1 within the precision of experiment. In this work, however, the dimensions of singly periodic

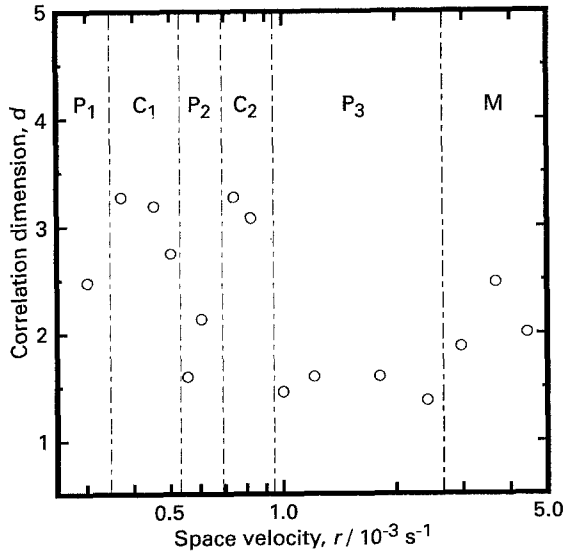

Fig. 6. Correlation dimension against space velocity.

regions are larger than 1 (about 1.5). The experimental data include some electrical noise and this noise causes an overestimation of the dimensions.

As mentioned before, these chaotic attractors are almost two-dimensional in the phase space while the correlation dimensions are $2.5 \sim 3.5$. Even if the influence of noise is taken into consideration, the correlation dimensions are still larger than 2. This result indicates that these strange attractors have fractal structures, and low dimensional, i.e. these chaotic motions generated by a few degrees of freedom. Hence, they correspond to deterministic chaos, not a stochastic behaviour which has a large number of degrees of freedom arising from fluctuations in the environment.

4. Concluding remarks

The following may be deduced:

(i) The single-peak periodic and the chaotic oscillations occur alternately with increasing the space velocity.

(ii) Two kinds of chaotic oscillations appear: chaotic oscillations with amplitudes varying irregularly, and chaotic mixing of large and small amplitudes.

(iii) Judging from the phase space portraits and their Poincaré sections, this chaotic behaviour is approximately two-dimensional.

(iv) The largest Lyapunov exponent and the correlation dimension are in a good agreement with each other, and they characterized periodic and chaotic oscillations clearly.

(v) The largest Lyapunov exponent and the correlation dimension indicate that the chaotic attractors are low dimensional and have fractal structures.

(vi) These results provide definitive evidence for the existence of deterministic chaos in this reaction at medium and high space velocity.

References

[1] R. A. Schmitz, K. R. Graziani and J. L. Hudson, *J. Chem. Phys.* **67** (1977) 3044.
[2] J. L. Hudson, M. Hart and D. Marinko, *ibid.* **71** (1979) 1601.
[3] J. L. Hudson and J. C. Mankin, *ibid.* **74** (1981) 6171.
[4] J. S. Turner, J. C. Roux, W. D. McCormick and H. L. Swinney, *Phys. Lett. A* **85** (1981) 9.
[5] J. C. Roux, J. S. Turner, W. D. McCormick and H. L. Swinney, *in* 'Nonlinear Problems: Present and Future', North-Holland, Amsterdam (1982) p. 409.
[6] S. K. Scott, *in* 'Chemical Chaos', Clarendon Press, Oxford (1991) p. 203.
[7] N. H. Packard, J. P. Crutchfield, J. D. Farmer and R. S. Shaw, *Phys. Rev. Lett.* **45** (1980) 712.
[8] F. Takens, *in* 'Lecture Notes in Mathematics', Vol. 898, Springer, Berlin (1981) p. 336.
[9] A. Wolf, J. B. Swift, H. L. Swinney and A. Vastano, *Physica* **16D** (1985) 285.
[10] P. Grassberger and I. Procaccia, *ibid.* **9D** (1983) 189.

Appendix: The mathematical theory of the phase space analysis

A brief description of the mathematical theory of phase analysis now follows.

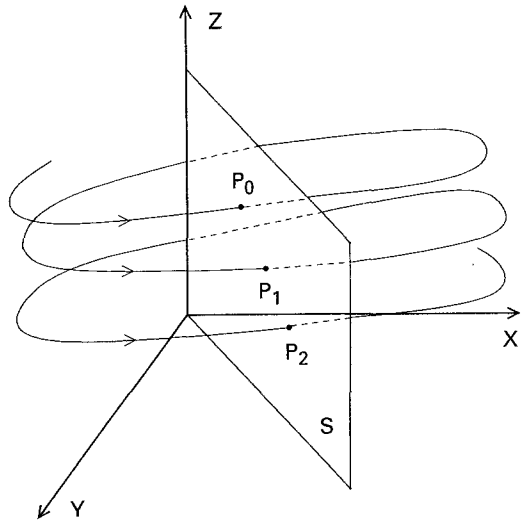

Fig. 7. Illustration of a Poincaré section.

A.1 *Poincaré sections*

It is assumed that an evolution of a dynamical system is described by a set of autonomous ordinary differential equations:

$$\frac{d}{dt}\boldsymbol{X}(t) = \boldsymbol{F}(\boldsymbol{X}(t)) \tag{A.1}$$

Here $\boldsymbol{X}$ is a vector of variables and $\boldsymbol{F}$ is a vector field over this space. A system of differential equations such as Equation A.1 is called a flow in the phase space. It can be rather easily understood to observe the points of intersection of the trajectory with a plane than directly studying the solution to Equation A.1 (Fig. 7). This plane is called the *Poincaré section* after French mathematician Henri Poincaré. The plane can be suitably chosen to be easily analysed. The transformation leading from one point to the next is a continuous mapping called the Poincaré map:

$$\boldsymbol{P}_n = T(\boldsymbol{P}_{n-1}) = T^2(\boldsymbol{P}_{n-2}) = \cdots = T^n(\boldsymbol{P}_0) \tag{A.2}$$

If the solution to Equation A.1 is unique, the point $\boldsymbol{P}_0$ determines $\boldsymbol{P}_1$, $\boldsymbol{P}_1$ determines $\boldsymbol{P}_2$, and so on. The Poincaré section replaces the differential equations (A.1) with the difference equations (A.2). Equations A.2 are not only easier to solve, but also reduce the number of coordinates by one.

A.2 *The largest Lyapunov exponent*

In a dynamical system described by Equation A.1, the evolution of a tangent vector δ in a tangent space at $\boldsymbol{X}(t)$ is represented by linearizing Equation A.1.

$$\frac{d}{dt}\delta(t) = \frac{\partial F}{\partial X}\delta(t) \tag{A.3}$$

The solution of Equation A.3 be obtained as

$$\delta(t) = \boldsymbol{A}\delta(0) \tag{A.4}$$

where $\boldsymbol{A}$ is a linear operator which maps tangent vector $\delta(0)$ to $\delta(t)$. Then the largest Lyapunov exponent which implies the exponentially fast diverging rate averaged over short time intervals of the tangent vector δ is defined as follows:

$$\lambda_{\max} = \lim_{N\to\infty} \frac{1}{N\Delta t} \sum_{i=1}^{N} \ln \frac{\| \delta_i(\Delta t) \|}{\| \delta_i(0) \|} \tag{A.5}$$

The largest Lyapunov exponent $\lambda_{\max}$ is zero for a limit cycle or a torus motion, although it is positive for chaos.

A.3 *The correlation dimension*

In a chaotic behaviour, there exists a spatial correlation of the positions of two points along the same trajectory that can be characterized through some function since all points are on the attractor. This function is called the correlation integral $\boldsymbol{C}(\epsilon)$ and defined as follows:

$$\boldsymbol{C}(\epsilon) = \frac{1}{N^2} \sum_{i\neq j} \boldsymbol{H}(\epsilon - \| \vec{x}_i - \vec{x}_j \|) \tag{A.6}$$

Here N is the number of the sampled data points, $\boldsymbol{H}$ is the Heaviside unit step function, ϵ is the radius of a hypersphere in the phase space. In a limited range of ϵ, the following power law is satisfied:

$$\boldsymbol{C}(\epsilon) \sim \epsilon^d \tag{A.7}$$

Then the correlation dimension d is defined as

$$d = \frac{\log \boldsymbol{C}(\epsilon)}{\log \epsilon}. \tag{A.8}$$